The Astrophysical Journal, 878:95 (14pp), 2019 June 20 https://doi.org/10.3847/1538-4357/ab1f65

Benchmark Rovibrational Linelists and Einstein A-coefficients for the Primordial Molecules and Isotopologues

Paulo H. R. Amaral[1], Leonardo G. Diniz[2], Keith A. Jones[3], Monika Stanke[4], Alexander Alijah[5], Ludwik Adamowicz[3,6], and José R. Mohallem[1]

[1] Laboratório de Átomos e Moléculas Especiais, Departamento de Física, ICEx, Universidade Federal de Minas Gerais, P. O. Box 702, 30123-970 Belo Horizonte, MG, Brazil; phramaral@gmail.com

[2] Coordenação de Ciências, Centro Federal de Educação Tecnológica de Minas Gerais, 30.421-169, Belo Horizonte, MG, Brasil; leogabriel@cefetmg.br

[3] Department of Chemistry and Biochemistry, The University of Arizona, Tucson, AZ 85721, USA; joneska@email.arizona.edu

[4] Institute of Physics, Faculty of Physics, Astronomy, and Informatics, Nicolaus Copernicus University, ul. Grudziądzka 5, Toruń, PL 87-100, Poland monika@fizyka.umk.pl

[5] Groupe de Spectrométrie Moléculaire et Atmosphérique, GSMA, UMR CNRS 7331, Université de Reims Champagne-Ardenne, U.F.R. Sciences Exactes et Naturelles, Moulin de la Housse B.P. 1039, F-51687 Reims Cedex 2, France; alexander.alijah@univ-reims.fr

[6] Interdisciplinary Center for Modern Technologies, Nicolaus Copernicus University, ul. Wileńska 4, Toruń, PL 87-100, Poland; ludwik@email.arizona.edu, rachid@fisica.ufmg.br

Received 2019 January 11; revised 2019 April 30; accepted 2019 May 2; published 2019 June 18

Abstract

Complete benchmark rovibrational energy linelists calculated for the primordial polar molecules of the universe, namely HD^+, HD, and the HeH^+ isotopologues, with accuracy up to 10^{-2} cm^{-1} for low-lying states, are presented. To allow for these calculations to be performed, new high-accuracy potential energy curves, which include the diagonal Born–Oppenheimer adiabatic corrections and the leading relativistic corrections, are determined. Also, a new approach for calculating non-adiabatic corrections involving an effective vibrational nuclear mass obtained based on the atoms-in-molecules theory is employed. The vibrational and rotational masses are taken as being different and dependent on the nuclear distance. Accurate dipole moment curves are calculated and used to generate lists of Einstein A-coefficients. The energy linelists and the sets of Einstein A-coefficients for HD are upgrades of previous calculations including quasibound states, while for HD^+ and HeH^+ and its isotopologues the present results represent significant improvement over the previous calculations. The results obtained here suggest that, with the inclusion of the non-adiabatic corrections, the accuracy limit at least for low-lying states might have been reached. Thus, further progress should involve accounting for even smaller effects such as the quantum-electrodynamics corrections. The present results represent the state-of-the-art of theoretical spectroscopy of the primordial polar molecules.

Key words: astrochemistry – molecular data – molecular processes

Supporting material: tar.gz file

1. Introduction

Two main factors, abundance and polarity, compete in the discussion of the spectroscopic role played by the smallest primordial molecules of the universe. This covers the period that started from their genesis when the temperature reached less than 4000 K (the recombination era) to the star formation at later times (Lepp et al. 2002). The homonuclear molecules H_2 and H_2^+ are expected to be the more abundant ones, but their spectroscopic contributions are negligible because they originate from quadrupole electric and/or dipole magnetic transitions. The ionic polar HD^+ and HeH^+ and its isotopologues, on the other hand, are expected to be less abundant but their spectroscopic contribution is much larger due to their much more intense electric dipole transitions. The slightly polar HD lies in terms of the spectroscopic contribution in between the above two groups of molecules due to its larger abundance (Galli & Palla 1998), but a small (though finite) spectroscopic contribution originating from its very small electric dipole moments. The HD and HeH^+ molecules play important roles in the study of interstellar matter and star- and planet-forming regions. Outside the scope of astrophysics, accurate calculations for HD^+ are of interest for metrology, in connection with the development of molecular clocks, as well as for the physics of fundamental constants, namely the improvement of the electron/proton mass ratio (Patra et al. 2018). Notably, HeH^+ has been detected very recently in space (Güsten et al. 2019).

But, in order to deepen the understanding of the cooling processes in the primordial universe and to study many other processes that became important in the later stages of the evolution of the universe, rovibrational linelists, as well as lists of Einstein A-coefficients, for these molecules, need to be determined with high accuracy. The more recent works that reported the data considered in the present work, namely energy linelists and Einstein A-coefficients, are Coppola et al. (2011) for HD^+, Pachucki & Komasa (2010) for HD, and Engel et al. (2005) for HeH^+ and its isotopologues. In Tung et al. (2012) some accurate transitions are reported for HeH^+ and its isotopologues. Pachucki & Komasa (2012) reported dissociation energies of the lowest rovibrational levels ($v \leqslant 5$ and $J \leqslant 14$) only for $^4HeH^+$. The corresponding total energy values taken from Coppola et al. (2011) and Engel et al. (2005) are tabulated in the website Exomol (Tennyson et al. 2016). Exomol databases for HD^+ and HeH^+ and isotopologues are mostly out-of-date. Pachuki and Komasa's databases for HD are very accurate but lack quasibound states, while their databases for $^4HeH^+$ (without other isotopologues) do not display all transitions and lack quasibound states and A-coefficients. Thus, the present work involving generation of state-of-the-art linelists, as well as complete sets of Einstein

A-coefficients for the key primordial systems, is very much in order.

Only a few groups have capabilities today to produce very accurate potential energy curves (PECs) for the electronic ground states of the molecules considered in the present work that include relativistic and diagonal Born–Oppenheimer (DBOC) corrections. In order to achieve an accuracy of at least $10^{-1}\,\mathrm{cm}^{-1}$, the inclusion of non-adiabatic corrections to the energy levels is imperative.

Non-adiabatic corrections are more difficult to obtain from ab initio calculations. One way to include these corrections is by using effective masses of the nuclei in determining rovibrational transitions. The effective masses simulate the electron dragging by the nuclei when the molecule is vibrating and/or rotating (Kutzelnigg 2007; Mohallem et al. 2011). The simple use of constant nuclear masses for the rotation calculations and atomic (or dissociation) masses for the vibration calculations already significantly improves the results. However, to reach the $10^{-1}\,\mathrm{cm}^{-1}$ accuracy in the calculations of the energy levels more sophisticated effective-mass models need to be employed. In these models, the effective vibrational and rotational masses need to depend on the inter-nuclear distance (i.e., the masses should be R-dependent).

In one of our previous papers (Diniz et al. 2018), the most accurate linelists and radiative cooling functions for the LiH isotopologues were calculated. In the calculations very accurate PEC and dipole moment curves (DMC) reported before (Diniz et al. 2016) were employed. The non-adiabatic corrections were obtained with the use of a constant reduced nuclear mass for rotations and a R-dependent mass taken from Diniz et al. (2015; obtained in valence-bond calculations) for vibrations.

In the present work, further progress in calculating PECs (Jones et al. 2016a), as well as a new procedure for calculating non-adiabatic corrections, are reported. The approach is used in state-of-the-art rovibrational calculations for the target molecules. The progress in the PEC calculations includes implementation of improved procedures for calculating the leading relativistic corrections. The progress in calculating the non-adiabatic effects includes implementation of a procedure based the atoms-in-molecules (AIM) core-valence partition of the electronic density (Amaral & Mohallem 2017). The partition allows for the determination of the fractions of the electron density that needs to be added to the nuclear masses to produce the effective vibrational reduced masses. Both implementations have allowed us to achieve the $10^{-1}\,\mathrm{cm}^{-1}$ accuracy in the transition energy calculations.

The present paper is organized as follows. Section 2 contains a brief discussion of the basic spectroscopy equations for calculating the rovibrational energy levels and A-coefficients. Section 3 describes the methodology used to calculate the PECs and DMCs. In Section 4 the AIM approach for calculating effective nuclear masses is discussed. In Section 5 the results for which comparison with available experimental and theoretical data is possible are presented. The complete set of the data calculated in this work are presented in the tar.gz package in the Appendix. The paper is concluded with a general discussion and a summary.

2. Basic Equations

For an electronic state well separate from other states (the so-called one-state approximation), Schrödinger's radial equation for a diatomic molecule is (Bunker & Moss 1977):

$$\left[-\frac{1}{2\mu_{\mathrm{vib}}}\frac{d^2}{dR^2}+E_e(R)+\frac{J(J+1)}{2\mu_{\mathrm{rot}}R^2}-E_{vJ}\right]\chi_{vJ}(R)=0, \quad (1)$$

where μ_{vib} and μ_{rot} are the vibrational and rotational reduced masses, respectively, $E_e(R)$ is the PEC, and E_{vJ} and χ_{vJ} are the eigenvalues and rovibrational wavefunctions of the quantum state characterized by the vibrational and rotational quantum numbers v and J. In the electronic calculations, in which the PEC is obtained, the nuclei are considered to have infinite masses (the Born–Oppenheimer (BO) approximation). To solve the above radial equation, Equation (1), the masses μ_{vib} and μ_{rot} are usually assumed to be the same and equal to the reduced mass of the nuclei. This assumption is not used in the present work because, as shown later in this work, the R-dependence of the masses is found to be crucial to improve the calculation accuracy. In highly accurate calculations, diagonal Born–Oppenheimer and relativistic corrections are typically added to the BO PEC before solving Equation (1). Once this equation is solved and a set of rovibrational wavefunctions and the corresponding energies is obtained, the Einstein A-coefficients (or dipole transition probabilities) are calculated using the DMC, $d(R)$, as

$$A_{v'J'v''J''}=\left(\frac{16\pi^3}{3\epsilon_0 h}\right)\frac{S(J',J'')}{2J'+1}\nu^3\,|\langle\chi_{v'J'}|d(R)|\chi_{v''J''}\rangle|^2, \quad (2)$$

where $S(J', J'')$ are the Hönl–London rotational intensity factors, ϵ_0 is the permittivity of vacuum, h is the Plank constant, and ν is the transition frequency. Here, the symbols (v', J') and (v'', J'') denote, respectively, the upper and lower rovibrational states between which a spontaneous transition occurs. For further details of the theoretical procedure the reader is referred to Diniz et al. (2016).

3. Potential Energy and DMCs

The present-day experimental high-resolution spectroscopy of small molecules has an accuracy of less than $10^{-2}\,\mathrm{cm}^{-1}$ (see, for example, Sprecher et al. 2010). Reaching similar accuracy in theoretical calculations is a serious challenge for theoreticians. The starting point for rovibrational calculations are usually highly accurate PECs obtained within the Born–Oppenheimer approximation. At this level, the accuracy of state-of-the-art curves is better that $0.002\,\mathrm{cm}^{-1}$ for each BO point (Tung et al. 2012), which results, without further corrections, in an accuracy of at most tenths of cm^{-1} for the rovibrational energy levels. The adiabatic correction (DBOC) amounts to about $10^2\,\mathrm{cm}^{-1}$ and contributes within 10^0–$10^1\,\mathrm{cm}^{-1}$ to the energy levels. Thus they must be included in the PECs. As demonstrated by Tung et al. (2012), these terms can be presently evaluated with an accuracy better than $0.0005\,\mathrm{cm}^{-1}$. The leading relativistic corrections for two electron systems (Kediziera et al. 2006) are about one order of magnitude smaller than the adiabatic correction, but when summed with the leading quantum-electrodynamics (QED) corrections they become more relevant with increasing vibrational quantum number v. The remaining differences between the calculated and the experimental levels are mainly due to non-adiabatic corrections.

The calculations performed in the present work are based on the new high accurate PECs presented in the tar.gz package Appendix. They were constructed by the variational minimization of the expectation value of the BO electronic Hamiltonian for each point of the PEC, as done in Tung et al. (2012). The electronic wavefunctions are expanded on a basis of explicitly correlated Gaussian functions (ECGs) with shifted centers. The functional form of the basis functions can be seen in Equation (2) in Pavanello et al. (2008). The optimization of the nonlinear parameters of the ECGs is carried out in a cyclic process as described in Jones et al. (2016b). This cyclic optimization of individual functions was shown to be effective for an all-particle ECG basis in non-Born–Oppenheimer calculations of diatomic molecules (Jones et al. 2016b), and proved effective in this work as well. The analytic expression of the gradient of the energy with respect to the nonlinear ECG parameters is employed to speed up the optimization (Pavanello et al. 2008). In the process of growing the basis set new functions are added to the basis as described in Jones et al. (2016a). This addition involves identifying a subset of the functions that have the greatest energy contribution. Next, these functions, called candidate functions, have their nonlinear parameters perturbed slightly, followed by optimization of their nonlinear parameters. After checking the optimized functions for linear dependence with themselves and with the functions already included in the basis set and eliminating the functions that cause the linear dependence, the new most contributing optimized candidate functions are included in the basis set.

In order to construct a PEC, a single point on the curve is first optimized. Usually this point corresponds to the equilibrium inter-nuclear distance. A new point in proximity to the optimized point is then selected and a procedure based on the Gaussian product theorem is used to shift the centers of the ECGs optimized for the first PEC point to the new point (Cencek & Kutzelnigg 1997). The nonlinear parameters of the ECGs of the new point are then re-optimized in the way previously mentioned. After the optimization of the ECG basis set is completed and the corresponding electronic energy and the wavefunction is calculated, the next PEC point is selected and its ECG basis set is generated and optimized. This is again followed by the energy and wavefunction calculations. The procedure continues until the whole PEC is calculated. The density of the points along the PEC is uneven—more dense in the range where PEC changes more and less dense for more linearly behaving parts of the PEC.

The calculations of the DBOCs for the various isotopologues are carried out as described in Tung et al. (2012) and Cencek & Kutzelnigg (1997). As pointed out, the accuracy of the calculations is about $0.0005\,\mathrm{cm}^{-1}$. The DBOCs are added to the PEC to generate PECs for different isotopologues.

The main improvement in the PECs in this work comes from including the leading relativistic corrections calculated with the newly derived algorithms involving expectation values of the operators representing the corrections in the electronic relativistic Breit-Pauli Hamiltonian (Bethe & Salpeter 1977). The relativistic corrections to the electronic energy include mass–velocity, one- and two-electron Darwin, orbit–orbit, and spin–spin corrections. The expectation values are calculated using the ECGs optimized for each PEC point. The details of the derivation and implementation of the algorithms are outlined in Stanke et al. (2016a, 2016b).

The HeH^+ DMC needed for the evaluation of the Einstein A-coefficients are generated in the same calculations where the energies and wavefunctions for the PEC points are determined. The DMC is the same for $^4HeH^+$ and its isotopologues. Details on the procedure followed here can be found in Diniz et al. (2016).

Computations of the isotopic dipole moments of HD^+ and HD demand special treatment. The DMC for HD^+ is also obtained here, by moving the center of coordinates to the center of mass of the nuclei. On the other hand, the DMC for the neutral HD is not performed here. Instead, it is taken from Pachucki & Komasa (2008), and is the same DMC used by Coppola et al. (2011). The new PECs and DMCs obtained for the particular grids of R used for the considered systems, are shown in the tar.gz package.

4. Non-adiabatic Effects on the Energy Levels

Along with the high accuracy of the PEC calculations, accounting for the non-adiabatic effects is crucial to improve the energy linelists. In cases of well-isolated ground electronic states weakly coupled to excited states, non-adiabatic corrections to the vibrational energy levels have their origin in the dragging of some fraction of the electron density by the nuclei when they rotate and vibrate (this effect contributes to the inaccuracy of the adiabatic model). Considering the physical nature of the non-adiabatic effect, it has been accounted for with increasing accuracy by taking the difference between the rovibrational energies calculated with nuclear masses and those obtained with empirical effective masses (Kutzelnigg 2007; Mohallem et al. 2011; Diniz et al. 2012) (the calculations with different masses are performed with the nuclear equation, Equation (1)). However, the empirical mass models introduced so far have been unable to account for the whole non-adiabatic effect.

In our recent paper, using the AIM theory developed within the iterative stockholder framework of Hirshfeld (1977) (SAIM), a core-valence electron separation (CVSAIM) model was introduced (Amaral & Mohallem 2017). The CVSAIM core electron densities are considered as moving along with the corresponding nuclei as these nuclei vibrate and rotate. These densities are R-dependent and should be added to the nuclear masses to determine the effective nuclear masses. These effective masses are to be used in the rovibrational nuclear equation to account for the non-adiabatic effects in the calculations of the rovibrational energy levels. As shown in Amaral & Mohallem (2017), this accounting for the non-adiabatic effects is so far the most accurate for the systems studied in that work. In the procedure there is no need to use any empirical scaling of the correction curves, such as, for example, the scaling used in Diniz et al. (2012).

The CVSAIM method for attributing effective masses to the nuclei can be outlined as follows. In the first step of the approach the one-electron density of the system, $\rho_{\mathrm{mol}}(r)$, is calculated for all PEC points. In the next step the CVSAIM density partition is performed for the density at each of the PEC points. The CVSAIM method is based on the AIM concept and the SAIM scheme introduce by Hirshfeld (1977). For example, let us take a diatomic molecule, AB, and let ρ_{A}^0 and ρ_{B}^0 be the densities of the isolated atoms. Let us call the sum of the two atomic densities, $\rho_{\mathrm{mol}}^0 = \rho_{\mathrm{A}}^0 + \rho_{\mathrm{B}}^0$, the promolecule density. Then, in the first-order approximation, the density of SAIM A,

ρ_A^1, is determined as

$$\rho_A^1 = \frac{\rho_A^0}{\rho_{mol}^0}\rho_{mol}, \quad (3)$$

with an analogous definition for ρ_B^1. The same procedure is followed for the nth-order approximation, namely,

$$\rho_A^n = \frac{\rho_A^{n-1}}{\rho_{mol}^{n-1}}\rho_{mol}. \quad (4)$$

The iterative procedure called ISA (iterated stockholder atoms, Lillestonen & Wheatley 2008), which is explained in Amaral & Mohallem (2017), allows determination of the SAIM densities of atoms A and B, ρ_A and ρ_B. The sum of these densities is the molecular density

$$\rho_{mol} = \rho_A + \rho_B. \quad (5)$$

SAIM introduces the concept of imitated atoms in the molecule, while CVSAIM introduces the idea that each SAIM has two different R-dependent parts, a core part that moves along with the nucleus when it vibrates and a valence part that does not participate in this motion. For the purpose of the present application of the SAIM approach, the core fraction of the CVSAIM for each atom must be identified. With this in mind, an effective one-electron potential for each AIM is constructed from the molecular density using the following procedure.

For each atomic center, say, atomic center A, its charge, $q(r_A)$, is obtained by numerical integration:

$$q(r_A) = \int \rho_{mol} d\tau, \quad (6)$$

where the integration is performed over a sphere of volume τ in which r varies from 0 to r_A. The effective potential, $V_A(r_A)$, is

$$V_A(r_A) = -\frac{Z_A + q(r_A)}{r_A}, \quad q(r_A) < 0, \quad (7)$$

where Z_A is the charge of nucleus A, and r_A ranges from 0 to the value that is determined from the condition: $V_A(r_A) = 0$. The same procedure is followed for atom B.

Once the molecular density is partitioned into the CVSAIM components, the core fraction of the electron density of CVSAIM A, $\rho_{A,c}$, is chosen as the part of the whole SAIM density preponderantly subject to the potential V_A, that is, corresponding to the region where V_A is more attractive than V_B (Figure 4 of Amaral & Mohallem (2017) illustrates this feature). The same procedure is followed to obtain the core fraction of the CVSAIM density of atom B, $\rho_{B,c}$. It should be noted that for homonuclear molecules the cores are easily identified as the non-superposed parts of the CVSAIM densities. Then, the superposing part of the densities correspond to the stationary density of the valence electrons (see Figure 1 in Amaral & Mohallem 2017).

The electronic masses to be added to the nuclear masses, in order to determine the effective nuclear masses, are obtained by numerical integration of the core part of the CVSAIM density for each atomic center. With that the effective mass of, for example, nucleus A, is:

$$m_{A,vib}(R) = m_A + m_e \int \rho_{A,c}(r, R) d\tau, \quad (8)$$

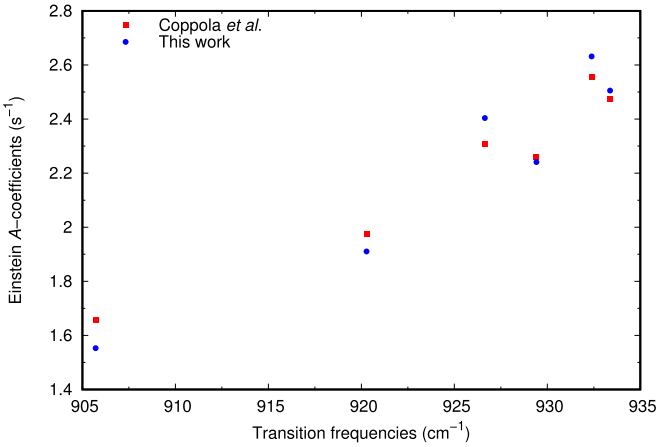

Figure 1. Comparison of the Einstein A-coefficients for the (18–16) band of the R-branch of HD^+.

where m_A is the mass of the bare nucleus A and m_e is the electron mass, with an analogous expression for $m_{B,vib}(R)$. Once $m_{A,vib}(R)$ and $m_{B,vib}(R)$ are determined for all grid points of the PEC, the effective vibrational reduced mass is calculated as

$$\mu_{vib}(R) = \frac{m_{A,vib}(R) m_{B,vib}(R)}{m_{A,vib}(R) + m_{B,vib}(R)}. \quad (9)$$

Vibrational energies that include the non-adiabatic corrections are obtained by solving the vibrational equation with the effective reduced mass of Equation (9). Either an algorithm that allows for the reduced mass to be R-dependent (Alijah & Duxbury 1990), or an algorithm that employs a constant reduced mass can be used, provided that, in the latter case, the masses are averaged over the vibrational states as

$$m_{A,v} = \int m_A(R) \chi_v(R)^2 dR, \quad (10)$$

as described in Mohallem et al. (2011), where $\chi_v(R)$ is the wavefunction for vibrational level v.

In order to obtain good-quality effective masses using the above-described approach, electronic densities are obtained using the GAMESS program package (Schmidt et al. 1993). The calculations are performed at the full-CI level with the cc-pV5Z basis set for HD and HD^+ and with the cc-pVQZ basis set for HeH^+. The inclusion of finite nuclear mass effects (Gonçalves & Mohallem 2004) in the calculations of the electronic energies and the corresponding wavefunctions, and the subsequent calculations of the CVSAIM from the electronic density, is not needed because the densities obtained from the BO calculations are not significantly different (Mohallem et al. 2011; Diniz et al. 2012).

The use of effective rotational masses is less important in the calculations of the rovibrational levels than the use of effective vibrational masses. So far, there has not been a physically motivated model for determining effective rotational masses such as the models used for determining effective vibrational masses. As the potential in rovibrational equation depends on the quantum number J, for a fixed J a model for determining a common vibrational and rotational reduced mass can be established. Also, an empirical approach to determine such a reduced mass can, perhaps, be used. The approach chosen here involves determining an effective reduced rotational mass

through an interpolation of R-dependent reduced mass, which at the limit of small R can be accurately approximated using the nuclear masses and at large R can be approximated using the atomic masses (Diniz et al. 2012). The reasoning behind such an approach is that, for low values of J, a good approximation is to use a constant rotational reduced mass equal to $\mu_{\rm rot}(R) = m_{\rm A} m_{\rm B}/(m_{\rm A} + m_{\rm B})$, since the length of the bond is affected little by the rotation. However, as the values of J become larger and the molecule rotates more vigorously, the bond stretches (to eventually break at dissociation) and the nuclear rotational reduced mass approaches the atomic (or dissociation) reduced mass. Thus, a parameterization of the rotational reduced mass can be considered that, near the equilibrium distance, becomes equal to the reduced mass obtained from the nuclear masses and near dissociation becomes equal to the reduced mass obtained from the atomic masses. Such a behavior of $m_{\rm A,rot}$ can be represented by the following formula:

$$m_{\rm A,rot}(R) = m_{\rm A} + a[1 - [1 + e^{\alpha(R-R_T)}]^{-1}]. \quad (11)$$

Here, a is the net number of electrons in each atomic fragment (for example, $a = 1$ for H_2, $a = \frac{1}{2}$ for H_2^+), while α and R_T, the turning-point parameters of the function, are empirical parameters. They are obtained for each system using the procedure described in Diniz et al. (2012). The effective, R-dependent rotational reduced mass in Equation (1) is then obtained using Equation (9) with the rotational masses of the nuclei determined as described above.

5. Transition Energies and Einstein A-coefficients

In this section, tables of the calculated transition energies for which experimental and previous theoretical data are available and tables of selected Einstein A-coefficients are presented. The complete linelists and Einstein A-coefficients data are shown in the tar.gz package. In the Appendix, extracts from the full material are presented for the $^3HeH^+$.

The rovibrational bound states are computed with the renormalized Numerov code that employs coordinate-dependent reduced masses (Alijah & Duxbury 1990). The numerical integration is performed within the R ranges and for the same R grids used in the PEC calculations. The parameters of the procedure are adjusted to achieve numerical convergence of $10^{-14}E_h$.

The energies of resonant (Q, quasibound) states are calculated with the LEVEL16 package (LeRoy 2017) modified to allow the use of different vibrational and rotational masses. As this code does not handle R-dependent masses, the effective vibrational and rotational masses are averaged, using Equation (10), over the wavefunctions obtained using nuclear masses in Equation (1).

5.1. HD^+ and HD

In the cooled primordial plasma and star environments rich in D atoms, HD^+ and HD could be formed by simple chemical reactions and ionization processes mostly discussed in Lepp et al. (2002), where their abundance at large redshifts are also discussed.

The generation of linelists for these species (polar and apolar) and their isotopologues is thus of great relevance to the study of the primordial plasma. Experimental energies for some transitions of the species can be obtained from Carrington et al. (1983) (for HD^+) and Chuang & Zare (1987) (for HD). On the theoretical side, while for the one-electron ion HD^+ quasi-exact values exist for some levels (Wolniewicz & Poll 1986; Balint-Kurti et al. 1990; Korobov 2006, 2008; Ishikawaa et al. 2012; Nakashima & Nakatsuji 2013; Nakashima et al. 2013), the most accurate full linelist seems to be that from Coppola et al. (2011). With the aim of calculating the radiative cooling function, they used the PEC and the DMC generated in Esry & Sadeghpour (1999) using an approach that resorts to a particular adiabatic formalism that generates isotopic electronic splitting instead of accounting for the ab initio DBOC.

Here, the most accurate PECs referred to in Section 3 corrected for DBOC and relativistic effects are used, and the results include non-adiabatic corrections obtained with the method described in Section 4. This yields a complete linelist for HD^+ that is likely the most accurate to date, and a very accurate full linelist for HD.

Table 1 presents pure vibrational transition energies for HD^+. The results are compared to quasi-exact results from Balint-Kurti et al. (1990). The improvement in comparison with the linelist presented in Coppola et al. (2011) is remarkable. The deviations between the present linelist and that of Coppola et al. (2011) of dozens of cm^{-1} can probably be attributed to the inaccuracy of their non-adiabatic corrections, as well as the procedure of using the adiabatic corrections taken from Esry & Sadeghpour (1999), which are not equivalent to the ab initio DBOC. On the other hand, the larger error that

Table 1
HD^+—Comparison between Calculated Vibrational Term Values and the Quasi-exact Ones Taken from Balint-Kurti et al. (1990)

$v \to 0$	Quasi Exact[a]	Coppola[b]	This Work
1	1912.9954	−1.1002	−0.0194
2	3729.8563	−1.5577	−0.0342
3	5453.4437	−0.7228	−0.0434
4	7086.2436	2.1810	−0.0530
5	8630.3773	7.7749	−0.0598
6	10087.6081	16.2648	−0.0602
7	11459.3429	27.3092	−0.0567
8	12746.6309	40.0948	−0.0469
9	13950.1552	53.5150	−0.0316
10	15070.2225	66.3806	−0.0145
11	16106.7442	77.5729	0.0117
12	17059.2135	86.1407	0.0360
13	17926.6727	91.3406	0.0656
14	18707.6747	92.6380	0.1124
15	19400.2309	89.6969	0.1655
16	20001.7545	82.3592	0.2218
17	20508.9903	70.6362	0.2841
18	20917.9639	54.7035	0.3717
19	21223.9914	34.9411	0.5376
20	21422.0170	11.7839	1.1761
21	21505.8596	−11.8565	8.2245
rms		55.4767	1.8211
rms*		59.478	0.107

Notes. Coppola: calculated term values from Tennyson et al. (2016). This work: term values calculated in this work. The two last columns contain the differences between calculated and quasi-exact term values. All data are in wavenumbers, cm^{-1}. rms* discards states with v larger or equal to 18, for which the average R approaches/exceeds the avoided-crossing region.
[a] Balint-Kurti et al. (1990).
[b] Coppola et al. (2011).

Table 2
Computed Transition Frequencies for HD^+ Compared (Observed–Calculated) with Experimental Data

		$P(J)$			$R(J)$		
$v'-v''$	J	Experiment[a]	Coppola[b]	This Work	Experiment[a]	Coppola[b]	This Work
1–0	0						
	1	1869.134	1.036	0.020			
	2	1823.533	0.978	0.021			
	3	1776.459	0.928	0.023			
2–1	0				1856.778	0.556	0.011
3–2	0				1761.616	−0.664	0.006
	1				1797.522	−0.433	0.005
	2	1642.108	−0.955	0.011	1831.083	−0.162	0.004
17–14	0				1813.852	23.954	−0.173
	1	1782.772	19.650	−0.169	1820.209	25.416	−0.173
	2				1820.199	26.306	−0.178
	3				1813.644	26.581	−0.182
	4				1800.358	26.224	−0.186
	5				1780.145	25.246	−0.191
17–15	1	1092.124	16.782	−0.115			
	2	1071.561	14.285	−0.115			
	3	1047.239	11.692	−0.114			
	5	987.917	6.688	−0.115			
	6	953.180	4.504	−0.117			
	7				1078.853	20.126	−0.149
18–16	0				926.490	29.362	−0.152
	1	901.565	25.509	−0.148	932.224	30.542	−0.156
	2	882.731	23.026	−0.150	933.213	31.124	−0.161
	3				929.247	31.063	−0.168
	4				920.100	30.340	−0.177
	5				905.519	28.963	−0.191
	6				885.218	26.979	−0.208
20–17	0				918.102	59.974	−0.927
	1	900.488	56.898	−0.889	915.476	60.207	−1.006
	2	880.668	54.212	−0.920	904.833	59.533	−1.145
	3				885.749	58.000	−1.388
21–17	0				998.533	83.009	−8.459
	1	984.330	80.537	−7.935	988.993	81.980	−9.553
	2				967.811	79.404	−11.235
	3	927.192	72.691	−9.543	…	…	…
	4	882.523	67.049	−11.223	…	…	…
22–17	0				1006.965	86.886	−14.720
	1	994.112	84.685	−14.605			
	2	969.530	81.191	−14.714			
	rms		44.994	6.120		44.790	4.434
	rms*		10.380	0.098		19.885	0.141

Notes. All units are cm^{-1}. rms* discards states with v larger or equal to 18, for which the average R approaches/exceeds the avoided-crossing region.
[a] Carrington et al. (1989).
[b] Coppola et al. (2011).

appears for higher states and affects both their and our calculations is most certainly due to an avoided crossing similar to that appearing in H_2^+ at $R \simeq 6$ au (Jiang et al. 2017). The error becomes particularly significant for vibrational levels with a v equal and larger than 18.

Table 2 presents energies of the rovibrational transitions of the P and R branches of HD^+ for which experimental values are available. The transitions are compared with the linelist taken from Coppola et al. (2011). The present results are clearly superior, with some low-lying transitions having an accuracy of less than $0.1\ cm^{-1}$.

Shen et al. (2012) resolved the hyperfine structure of the fundamental rotational transition (0,0)–(0,1), which turns to extend over $+0.0100$ and $-0.0233\ cm^{-1}$ around the spinless theoretical value of $43.861201872\ cm^{-1}$ from Korobov (see reference 23 in Shen et al. 2012 and Korobov 2006, 2008). Remarkably, the present result for this transition, $43.862873992\ cm^{-1}$, deviates by only $0.0017\ cm^{-1}$ from Korobov's result.

Carrington et al. (1992) performed measurements and accurate calculations (within $0.001\ cm^{-1}$) for some transitions between bound and quasibound states. In Table 3 the performances of the two linelists are compared for these transitions, showing again the superiority of the present results. A look to the rms deviations shows that the quality of the present results is kept for the quasibound states.

For applications in astrophysics it is important that the linelist include the quasibound states, which are frequently necessary for understanding many physical and chemical molecular properties. On the other hand, some transitions involving these states have lifetimes that are too small due to

Table 3
Bound to Quasibound Computed Transition Frequencies for HD^+ Compared (Observed–Calculated) with Experimental Data

		$P(J)$			$R(J)$		
v'–v''	J	Experiment[a]	Coppola[b]	This Work	Experiment[a]	Coppola[b]	This Work
1–0	44				1022.667	−0.202	0.137
2–1	42				1010.735	−0.161	0.109
3–2	40				999.144	−0.108	0.081
4–3	38				986.392	−0.047	0.054
13–10	24	1087.426	0.052	0.004			
14–11	22	1047.787	0.145	−0.050			
14–12	20				1034.779	0.426	−0.043
15–13	18				949.049	0.660	−0.118
15–12	20	994.682	0.211	−0.132			
17–15	7				1078.853	20.126	−0.149
	8				1051.735	17.916	−0.156
	10				978.917	12.766	−0.183
	11				932.229	10.139	−0.211
16–13	18	926.176	0.284	−0.265			
19–16	6	1036.961	27.789	−0.398			
	7	983.693	23.9367	−0.456			
	rms		14.974	0.276		9.962	0.134

Notes. All units are cm^{-1}.
[a] Carrington et al. (1992).
[b] Coppola et al. (2011).

Table 4
Computed Transition Frequencies for HD Compared with Experimental Data (Observed–Calculated)

		$P(J)$			$R(J)$		
v'–v''	J	Experiment[a]	Pachucki[b]	This Work	Experiment[a]	Pachucki[b]	This Work
1–0	0				3717.532	−0.0003	0.048
	1	3542.932	−0.0005	0.055	3798.455	0.0035	0.050
	2	3450.463	−0.001	0.060	3874.357	0.0038	0.049
	3	3355.361	−0.009	0.058	3944.720	0.0011	0.047
	4				4009.088	0.0012	0.049
4–0	0				13551.065	−0.0117	0.003
	1	13387.646	−0.0149	0.000	13609.664	−0.0121	0.002
	2	13283.993	−0.0145	0.007	13652.215	−0.0032	0.012
	3				13678.322	−0.0039	0.014
5–0	0				16486.537	−0.0115	−0.090
	1	16326.791	−0.0138	−0.093	16537.816	−0.0017	−0.087
	2	16219.473	−0.0063	−0.082	16569.404	0.0044	−0.088
	3				16581.008	0.0501	−0.050
	rms		0.0105	0.060		0.0152	0.054

Notes. All units are cm^{-1}.
[a] Chuang & Zare (1987).
[b] Pachucki & Komasa (2010).

predissociation Carrington et al. (1992, 1993). For the convenience of the reader, in the tar.gz package these states are separated and located at the bottom of the tables.

Moving to HD, the reference work from Wolniewicz (1995) displays very accurate energy values and transitions, though no attempt to generate the full linelist or complete set of Einstein A-coefficients has been made. An old linelist from Abgrall et al. shows an attempt to include electric quadrupole transitions but presents large deviations of about 1 cm^{-1} in the transitions. The more recent linelist for HD is from Pachucki & Komasa (2010), with the full data set displayed in the HITRAN Database (Rothman et al. 2017). It includes non-adiabatic, relativistic, QED, and smaller effects, thus presenting extremely accurate transition values within 0.01 cm^{-1}, but no transitions involving quasibond states.

Table 4 shows energies of some rovibrational transitions obtained here compared with experimental values, resulting in a very good rms deviation of 0.05 cm^{-1}, which is consistent with the other applications despite being worse than that in Pachucki & Komasa (2010). It is not easy to explain this difference at this level of accuracy. Apparently, their quasi-exact approach for H_2 bound states in Pachucki & Komasa (2009) is easier to be extend

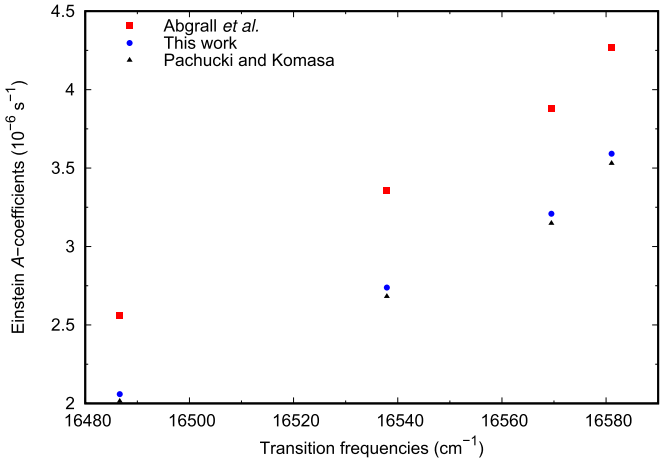

Figure 2. Comparison of the Einstein A-coefficients for the (5–0) band of the *R*-branch of HD.

to HD (Pachucki & Komasa 2010) with a perturbative approach. Furthermore, some other factors influence the observed differences besides the inclusion of QED corrections. While the present non-adiabatic corrections are fully based on effective nuclear masses taken from the electronic density, part of the non-adiabatic corrections in Pachucki & Komasa (2010) is in the potential, while their vibrational effective mass assumes "non-physical" values larger than the atomic mass, namely the sum of the masses of the atoms, for some values of *R*. On the other hand, the present work includes quasibound states in the linelist as well as A-coefficients, absent in Pachucki & Komasa (2010).

The full lists of Einstein A-coefficients for HD^+ and HD can be found in the tar.gz package. Figures 1 and 2 display selected examples concerning comparison with previous calculations. It has been shown that the A-coefficients are affected little by the non-adiabatic effects (Diniz et al. 2016), but they are sensitive to the quality of the wavefunctions and energies, so that they are expected to differ from the previously reported values. Figure 1 compares the present values of A-coefficients for the (18–16) band of the R-branch of HD^+ with those from Coppola et al. (2011). Small but significant differences can be seen. For the (5–0) band of the R-branch of HD (Figure 2), the present values are compared with the data from Abgrall et al. (1982) and Pachucki & Komasa (2010). As expected, the present transition probabilities are very close but not exactly equal to those from Pachucki & Komasa (2010). The calculation of the high-resolution spectroscopic parameters of the studied molecules should profit from the accuracy improvements implemented in the present work.

5.2. HeH^+ and Isotopologues

HeH^+ is the smallest heteronuclear molecule and is supposed to be the first molecule formed in the primordial universe. Its recent discovery in space represents a spectacular progress for the field of molecular astrophysics (Güsten et al. 2019). In Roberge & Dalgarno (1982) one can find a study of the formation and destruction of HeH^+ in astrophysical plasmas. There are six stable isotopologues of the system, $^4HeH^+$, $^4HeD^+$, $^4HeT^+$, $^3HeH^+$, $^3HeD^+$, and $^3HeT^+$ with the first being the most prevalent. Some sets of rovibrational and pure rotational transitions obtained using different experimental techniques were collected (Coxon & Hajigeorgiou 1999) and have been used for comparison by theoreticians. In this work they are used too.

Table 5
Rotation-vibration Frequencies for $^4HeH^+$ (Observed–Calculated), Pachucki & Komasa (2012), and Present Work without and with QED, Compared with Experimental Data

ν	J	Experiment[a]	Pachucki	This Work	This Work QED
1	1	67.053	0.004	−0.002	−0.001
	2	200.769	0.010	−0.007	−0.005
	3	400.379	0.020	−0.013	−0.008
	4	664.732	0.032	−0.025	−0.016
	5	992.324	0.051	−0.034	−0.021
	6	1381.287	0.067	−0.051	−0.033
	7	1829.447	0.093	−0.064	−0.040
2	0	2910.958	0.006	−0.010	0.007
	1	2972.574	0.009	−0.013	0.005
	2	3095.427	0.014	−0.017	0.003
	3	3278.761	0.023	−0.024	−0.002
	4	3521.456	0.036	−0.032	−0.007
	5	3822.029	0.050	−0.044	−0.015
	6	4178.661	0.067	−0.057	−0.024
	7	4589.196	0.079	−0.079	−0.041
	8	5051.199	0.107	−0.089	−0.046
rms			0.052	0.044	0.023

Note. All units are cm^{-1}.
[a] Perry et al. (2014).

Comparison of the present results is made in Table 5 with some recent experimental data from Perry et al. (2014), obtained with high precision sub-Doppler infrared spectroscopy, as well as to the $^4HeH^+$ calculations in Pachucki & Komasa (2012). It is notable that the present results are systematically larger while, in contrast, Pachucki & Komasa (2012) values are systematically lower than the experimental results. Since Pachucki & Komasa (2012) use the same approach of their application to HD, this becomes an opportunity to check our supposition in the previous section that the differences of the two approaches lye mainly in the different non-adiabatic corrections. With this goal, the QED corrections from Pachucki & Komasa (2012) are added to the present PEC and a corresponding set of transition energies is produced, shown in the last column of Table 5. The improvement in the accuracy of the present results in the second decimal place in cm^{-1} is notable, but only a few values become lower than the experimental ones. The differences from Pachucki & Komasa (2012) diminish but still keep in the second decimal place thus reinforcing our supposition that their main source is the different non-adiabatic approaches and that the superior performance of Pachucky and Komasa's method for HD is probably due to its fitness to this particular system. Note also that, different from the HD case, even the present results without QED contributions are more accurate than those in Pachucki & Komasa (2012). Thus, for further comparison, only the works displaying large number of transitions and different isotopologues are kept.

Contrary to the previously described systems, very accurate linelists exist for HeH^+ and its isotopologues such that the present results obtained with the new PECs and the *R*-dependent vibrational masses can be gauged. The present results are compared with two previous calculations. The PEC from Kolos & Peek (1976) corrected for DBOC in Bishop & Cheung (1979), but without the relativistic corrections, was used in the rovibrational calculations performed in Engel et al. (2005). To simulate non-adiabatic effects they tried various effective

reduced nuclear masses, but in the end chose the dissociation reduced mass, as it produced results that agreed best with the experimental results. Here, only their results obtained with the latter choice of reduced mass are used for comparison. While their results for $^4HeH^+$ are explicitly presented in Engel et al. (2005), those for the other isotopologues are found in the ExoMol compilation (Tennyson et al. 2016). In Tung et al. (2012) a very accurate HeH^+ PEC from Pachucki (2012) augmented with DBOCs, but without the relativistic corrections, was used in the calculations. To account for non-adiabatic effects, they also used a constant vibrational reduced mass obtained by the minimization of the difference between their transition energy of the lowest pure vibrational transition of $^4HeH^+$ and that of their previous non-BO calculation. The difference of their lowest calculated transition and the experimental transition then becomes zero. This optimized reduced mass was also used for the other states without reoptimization.

The procedure of Tung et al. (2012) improved upon the results of Engel et al. (2005) by about one order of magnitude. An analysis of Table 1 or 2 in Engel et al. (2005) shows clearly that the significant differences between the two sets of results cannot be attributed to only the non-adiabatic corrections, but are result of the improvements of both the BO PEC and the DBOC by Tung et al. The present PECs are further improved relative to the PECs of Tung et al. through the inclusion of relativistic corrections.

The comparison presented in Table 6 for purely rotational transitions of $^4HeH^+$ provides some interesting information. One can see that the present results and those of Engel et al. and Tung et al. have approximately the same quality, as determined by comparing the rms deviations. In fact, it becomes clear that any reasonable rotational mass works well and the inclusion of the relativistic corrections (this work) changes the results expressed in cm^{-1} only at the third figure after the decimal point.

The most significant improvement of the results is achieved in the present approach due to the use of the improved vibrational masses, as shown in Tables 7–10. For $^4HeH^+$ (Table 7) and for $^4HeD^+$ (Table 8), for which the most comprehensive comparison can be performed due to a large number of experimental transitions, the present rms deviations are one order of magnitude smaller, on average, than those of Engel et al., and about half of those of Tung et al. For $^3HeH^+$ (Table 9) and $^3HeD^+$ (Table 10) the improvement is not as impressive, though still noticeable. This mostly results from the small number of available experimental transition energies that can be used in the comparison.

Table 6
Computed Pure Rotational Transition Frequencies for $^4HeH^+$ (Observed–Calculated), Engel et al. (2005), Tung et al. (2012), and the Present Work, Compared with Experimental Data

v	J''	J'	Experiment	Engel	Tung	This work	
0	0	1	67.053[a]	0.002	−0.001	−0.002	
	1	2	133.717[a]	0.003	−0.002	−0.004	
	6	7	448.160[b]	0.016	−0.006	−0.012	
	10	11	657.221[c]	0.005	−0.016	−0.022	
	11	12	701.317[c]	0.013	−0.009	−0.014	
	12	13	741.706[c]	0.007	−0.014	−0.018	
	13	14	778.224[c]	0.002	−0.018	−0.022	
	14	15	810.708[c]	−0.005	−0.023	−0.026	
	15	16	839.010[c]	−0.008	−0.027	−0.027	
	16	17	862.984[c]	−0.011	−0.028	−0.027	
	17	18	882.475[c]	−0.015	−0.032	−0.028	
	18	19	897.334[c]	−0.005	−0.022	−0.015	
	20	21	912.242[c]	−0.012	−0.028	−0.016	
	21	22	911.704[c]	−0.011	−0.028	−0.012	
	23	24	891.888[d]	−0.024	−0.035	−0.002	QB
	24	25	870.298[d]	−0.025	−0.038	−0.005	QQ
	25	26	837.180[d]	−0.042	−0.038	0.007	QQ
1	10	11	598.829[c]	0.009	−0.016	−0.025	
	11	12	637.767[c]	0.014	−0.014	−0.023	
	12	13	672.989[c]	0.018	−0.103	−0.019	
	13	14	704.270[c]	0.009	−0.022	−0.029	
	14	15	731.430[c]	0.012	−0.019	−0.024	
	15	16	754.235[c]	0.007	−0.022	−0.026	
	16	17	772.464[c]	0.007	−0.018	−0.020	
	17	18	785.837[c]	0.009	−0.013	−0.012	
	18	19	793.997[c]	−0.003	−0.019	−0.015	
	19	20	796.490[c]	−0.010	−0.019	−0.012	
	20	21	792.616[d]	−0.020	−0.021	−0.010	QB
	21	22	781.245[e]	−0.042	−0.033	−0.008	QQ
	22	23	760.340[d]	−0.033	−0.022	0.003	QQ
	23	24	724.933[c]	−0.063	−0.016	0.015	
2	13	14	627.320[c]	0.002	−0.014	−0.022	
	14	15	648.324[c]	0.005	−0.011	−0.018	
	15	16	664.559[c]	0.003	−0.014	−0.020	
	16	17	675.609[c]	0.003	−0.013	−0.016	
	17	18	680.895[c]	−0.001	−0.014	−0.015	
	18	19	679.586[c]	−0.011	−0.016	−0.014	
	19	20	670.340[c]	−0.023	−0.012	−0.005	
	20	21	650.613[d]	−0.034	0.007	0.008	QB
	rms[f]			0.015	0.026	0.019	
	rms[g]			0.019	0.026	0.018	

Notes. QB denotes transitions between a quasibound and a bound state and QQ denotes transitions between two quasibound states. All units are cm^{-1}.
[a] Matsushima et al. (1997).
[b] Liu et al. (1987).
[c] Liu & Davies (1997a).
[d] Liu & Davies (1997b).
[e] Hoyland (1967).
[f] rms calculated neglecting QB and QQ transitions.
[g] rms calculated including QB and QQ transitions.

6. Discussion

Present-day experimental spectroscopy of primordial molecules has accuracy better than $10^{-2}\,cm^{-1}$. Experimental data, however, are limited to few transitions and need to be supplemented with theoretical computations of high accuracy, which are fundamental for those working with molecular astrophysics and cosmology.

Once very accurate BO PECs (PESs) are calculated, they can be augmented by a hierarchy of the corrections that make the calculation of the rovibrational levels more accurate. These corrections are: (i) adiabatic (DBOC; changing the transition energies by a few cm^{-1}), (ii) non-adiabatic (changing the results of tenths to few units of cm^{-1}), and (iii) relativistic plus QED (affecting the results by fractions of cm^{-1}). While DBOC, relativistic, and QED corrections are directly included in the PECs, the non-adiabatic corrections are usually included at the level of the nuclear equation that is solved for the rovibrational energies. Furthermore, the relativistic and QED corrections can be positive or negative, depending on the rovibrational quantum numbers. It is possible that some results appearing in the linelists may be very close to the experiment, but others may be quite inaccurate. This problem can only be overcome using truly accurate non-adiabatic corrections. Corrections due to rotational masses also amount for about $10^{-1}\,cm^{-1}$ and can be reliably evaluated with an empirical procedure. The major effect that needs to be accounted for in order to reach the point

Table 7
Computed Rovibrational Transition Frequencies for $^4HeH^+$ (Observed–Calculated), Engel et al. (2005), Tung et al. (2012), and the Present Work, Compared with Experimental Data

		P(*J*)				*R*(*J*)				
v'–v''	*J*	Experiment	Engel	Tung	This Work	Experiment	Engel	Tung	This Work	
1–0	0					2972.573[a]	−0.213	−0.061	−0.014	
	1	2843.903[a]	−0.216	−0.060	−0.010	3028.375[a]	−0.212	−0.060	−0.014	
	2	2771.806[a]	−0.215	−0.056	−0.005	3077.992[a]	−0.216	−0.061	−0.017	
	3	2695.050[a]	−0.218	−0.053	−0.001	3121.077[a]	−0.220	−0.061	−0.019	
	4	2614.030[a]	−0.223	−0.051	0.001	3157.297[a]	−0.223	−0.060	−0.020	
	5	2529.134[b]	−0.228	−0.048	0.004	3186.337[b]	−0.230	−0.062	−0.023	
	6	2440.742[b]	−0.232	−0.044	0.007	3207.909[b]	−0.226	−0.064	−0.028	
	7					3221.752[b]	−0.228	−0.060	−0.025	
	9	2158.140[c]	−0.240	−0.032	0.015					
	10	2059.210[c]	−0.238	−0.029	0.016					
	11	1958.388[c]	−0.234	−0.027	0.016					
	12	1855.905[d]	−0.233	−0.029	0.011					
	13	1751.971[d]	−0.221	−0.025	0.011					
2–1	0					2660.284[e]	−0.017	−0.063	−0.024	
	1	2542.531[e]	−0.017	−0.063	−0.021	2710.566[e]	−0.021	−0.063	−0.026	
	2	2475.814[e]	−0.019	−0.062	−0.019	2754.624[b]	−0.031	−0.067	−0.031	
	3					2792.110[b]	−0.039	−0.068	−0.034	
	4					2822.683[b]	−0.047	−0.066	−0.034	
	5	2248.854[c]	−0.028	−0.047	−0.002	2846.009[b]	−0.060	−0.067	−0.037	
	6	2165.485[c]	−0.040	−0.046	−0.002	2861.786[b]	−0.053	−0.061	−0.033	
	7	2078.841[c]	−0.067	−0.048	−0.003	2869.690[b]	−0.079	−0.069	−0.043	
	8	1989.251[c]	−0.069	−0.042	0.002	2869.478[b]	−0.062	−0.041	−0.017	
	9	1896.992[d]	−0.092	−0.047	−0.004					
	10	1802.349[d]	−0.105	−0.043	−0.001					
	11	1705.543[d]	−0.117	−0.036	0.003					
	19	862.529[f]	−0.156	0.026	0.035					
	20	745.624[f]	−0.158	0.028	0.032					
3–2	4					2484.912[c]	−0.039	−0.053	−0.028	
	5	1966.356[c]	−0.023	−0.062	−0.022	2501.941[c]	−0.045	−0.053	−0.030	
	6					2511.188[c]	−0.055	−0.054	−0.033	
	8					2504.914[c]	−0.076	−0.046	−0.028	
	9					2488.632[c]	−0.083	−0.043	−0.027	
	17	833.640[f]	−0.147	0.001	0.020					
	18	719.769[f]	−0.158	0.019	0.034					
5–4	11	901.963[f]	−0.102	−0.029	0.012					
	12	807.806[f]	−0.127	−0.035	0.005					
6–5	8	863.378[f]	−0.091	−0.050	0.001					
	9	782.925[f]	−0.093	−0.038	0.013					
	12					979.904[g]	−0.248	0.065	0.050	QB
7–6	4	817.337[f]	−0.172	−0.020	0.040					
	5	760.367[h]	−0.200	−0.039	0.022					
7–5	12	938.200[i]	0.136	0.095	0.161	QB				
	rms[j]		0.163	0.042	0.017		0.140	0.060	0.028	
	rms[k]		0.162	0.045	0.033		0.146	0.060	0.029	

Notes. QB denotes transitions between a quasibound and a bound state. All units are cm^{-1}.
[a] Bernath & Amano (1982).
[b] Crofton et al. (1989).
[c] Purder et al. (1992).
[d] Tolliver et al. (1979).
[e] Blom et al. (1987).
[f] Liu & Davies (1997a).
[g] Carrington et al. (1983).
[h] Hoyland (1967).
[i] Carrington et al. (1981).
[j] rms calculated neglecting QB transitions.
[k] rms calculated including QB transitions.

at which relativistic, QED, and rotational-mass corrections are relevant is the proper accounting for corrections to the vibrational masses.

In the present work, an improved procedure for determining vibrational masses is introduced. The procedure uses ab initio electronic densities and overcomes the problem of heuristically

Table 8
Computed Rovibrational Transition Frequencies for $^4HeD^+$ (Observed–Calculated), Engel et al. (2005), Tung et al. (2012), and the Present Work, Compared with Experimental Data

		P(*J*)				*R*(*J*)				
v'–v''	*J*	Experiment	Engel	Tung	This work	Experiment	Engel	Tung	This work	
1–0	0					2348.628[a]	−0.184	−0.069	−0.039	
	1	2269.812[a]	−0.183	−0.062	−0.031	2384.108[a]	−0.180	−0.066	−0.037	
	2					2416.780[a]	−0.181	−0.069	−0.040	
	3	2181.432[a]	−0.191	−0.061	−0.029	2446.518[a]	−0.185	−0.072	−0.044	
	4	2134.011[b]	−0.198	−0.063	−0.031	2473.202[a]	−0.184	−0.071	−0.044	
	5	2084.633[b]	−0.202	−0.060	−0.029	2496.703[a]	−0.191	−0.075	−0.049	
	6					2516.917[a]	−0.191	−0.075	−0.049	
	7					2533.732[a]	−0.193	−0.075	−0.050	
	8	1926.132[b]	−0.212	−0.052	−0.021	2547.048[a]	−0.196	−0.075	−0.051	
	9					2556.772[a]	−0.188	−0.074	−0.051	
	10					2562.812[a]	−0.186	−0.075	−0.053	
2–1	1	2088.030[b]	−0.054	−0.069	−0.040					
	3					2252.028[b]	−0.050	−0.069	−0.043	
	4	1959.756[b]	−0.055	−0.056	−0.026					
	5					2297.086[b]	−0.057	−0.072	−0.048	
3–2	4					2078.586[b]	−0.004	−0.061	−0.037	
	5					2096.816[b]	−0.021	−0.070	−0.046	
	8					2131.027[b]	−0.056	−0.072	−0.050	
4–3	9					1920.660[b]	−0.029	−0.061	−0.037	
	12					1899.333[b]	−0.060	−0.055	−0.033	
6–4	22	1088.373[c]	−0.405	0.091	0.085	QB				
6–5	20					1003.329[c]	−0.263	0.066	0.041	QB
7–5	20	944.720[c]	−0.429	0.100	0.103	QB				
13–9	4					1073.475[c]	0.298	−0.013	0.158	QB
	6	911.705[c]	0.381	−0.023	0.159	QB				
	rms[d]		0.169	0.061	0.030		0.149	0.070	0.045	
	rms[e]		0.263	0.067	0.070		0.167	0.068	0.056	

Notes. QB denotes transitions between a quasibound and a bound state. All units are cm^{-1}.
[a] Crofton et al. (1989).
[b] Purder et al. (1992).
[c] Carrington et al. (1983).
[d] rms calculated neglecting QB transitions.
[e] rms calculated including QB transitions.

Table 9
Computed Rovibrational Transition Frequencies for $^3HeH^+$ (Observed–Calculated), Engel et al. (2005), Tung et al. (2012), and the Present Work, Compared with Experimental Data

		P(*J*)				*R*(*J*)				
v'–v''	*J*	Experiment	Engel	Tung	This work	Experiment	Engel	Tung	This work	
1–0	0					3060.433[a]	−0.271	−0.080	−0.037	
	1	2923.680	−0.279	−0.078	−0.033	3119.405[a]	−0.268	−0.082	−0.040	
	2	2846.775	−0.281	−0.072	−0.026	3171.549[a]	−0.266	−0.083	−0.043	
	3	2764.768	−0.287	−0.073	−0.026	3216.468[a]	−0.265	−0.084	−0.047	
	4	2678.113	−0.290	−0.069	−0.023	3253.785[a]	−0.267	−0.088	−0.052	
	5	2587.243	−0.296	−0.068	−0.023	3283.156[a]	−0.258	−0.086	−0.053	
	6	2492.591	−0.298	−0.064	−0.020	3304.247[a]	−0.254	−0.088	−0.057	
	7					3316.761[a]	−0.257	−0.088	−0.059	
6–5	11					981.322[b]	−0.208	0.123	0.096	QB
	rms[c]		0.289	0.071	0.026		0.263	0.085	0.049	
	rms[d]						0.258	0.090	0.056	

Notes. QB denotes transitions between a quasibound and a bound state. All units are cm^{-1}
[a] Crofton et al. (1989).
[b] Carrington et al. (1983).
[c] rms calculated neglecting QB transitions.
[d] rms calculated including QB transitions.

Table 10
Computed Rovibrational Transition Frequencies for $^3HeD^+$ (Observed–Calculated), Engel et al. (2005), Tung et al. (2012), and the Present Work, Compared with Experimental Data

		$P(J)$				$R(J)$				
v'–v''	J	Experiment	Engel	Tung	This Work	Experiment	Engel	Tung	This Work	
1–0	1	2378.374[a]	−0.219	−0.079	−0.053	2504.487[a]	−0.213	−0.089	−0.065	
	2					2540.161[a]	−0.214	−0.094	−0.071	
	3	2280.081[a]	−0.237	−0.083	−0.058	2572.388[a]	−0.211	−0.094	−0.071	
	4					2601.007[a]	−0.214	−0.098	−0.076	
6–5	18					1034.144[b]	−0.289	0.145	0.185	QB
7–5	18	995.415[b]	−0.463	0.207	0.253	QB				
	rms[c]		0.228	0.081	0.056		0.213	0.094	0.071	
	rms[d]		0.326	0.137	0.153		0.230	0.106	0104	

Notes. QB denotes transitions between a quasibound and a bound state. All units are cm^{-1}.
[a] Crofton et al. (1989).
[b] Carrington et al. (1983).
[c] rms calculated neglecting QB transitions.
[d] rms calculated including QB transitions.

choosing the masses. As shown in the present work, it allows for reaching high accuracy in the calculation of the rovibrational transitions. Consequently, benchmark linelists and Einstein A-coefficients have been obtained. The calculations have made use of new very accurate potential energy and DMCs. The results show that the limits for the quality of the PECs and for the adiabatic and non-adiabatic corrections might have been reached, at least for low-lying states. Furthermore, there is no need for any empirical adjustment of the masses so they can expected to be good for general use.

Contrary to HD^+ and HD, the calculations of Coppola et al., Tung et al., and Engel et al. for HeH^+ are very accurate (particularly those of Tung et al.). Thus, the improvement of the HeH^+ results achieved in the present work is clearly due to better vibrational masses. However, to reach the accuracy of $10^{-2}\,cm^{-1}$, the relativistic and QED corrections become relevant. Particularly, the QED effects that increase with increasing v and J (Komasa et al. 2011) become important. This explains the remaining deviations between the present results and the experiment. It should be noted that transition energies involving higher states can be subject to error compensation that needs to be assessed and understood. In any event, the quality of the present results concerning the studied charged and neutral molecular systems is likely state-of-the-art.

J.R.M. acknowledges the CNRS for a one month invited scientist position at the University of Reims Champagne-Ardenne in 2018. Support from the Brazilian agencies CNPq and CAPES is also acknowledged. This work was also supported in part by funds from the Polish National Science Centre granted on the basis of Decision no. DEC-2013/10/E/ST4/00033.

Appendix
Supplementary Tabular Data Sets

Twenty nine tables are supplied, containing data for $^3HeH^+$, $^4HeH^+$, $^3HeD^+$, $^4HeD^+$, HD^+, and HD calculated with effective masses. These data are provided in plain format in a tar.gz package.

Table 11
Potential Energy Curve for $^3HeH^+$

R (a.u.)	Energy (a.u.)
0.3500	−0.6636438612
0.4000	−1.2262242865
0.4500	−1.6362141802
0.5000	−1.9418274958
0.5500	−2.1735816512
0.6000	−2.3516580651
0.6500	−2.4898769615
0.7000	−2.5979773598
0.7500	−2.6829874901
0.8000	−2.7500815723

Table 12
Dipole Moment Curve for $^3HeH^+$

R (a.u.)	Dipole (a.u.)
0.3500	0.0476670167
0.4000	0.0591198908
0.4500	0.0719194239
0.5000	0.0860850194
0.5500	0.1016275588
0.6000	0.1185506199
0.6500	0.1368513598
0.7000	0.1565212256
0.7500	0.1775465621
0.8000	0.1999092100

Example data for the $^3HeH^+$ (potential energy and DMCs, rovibrational energy values, P-branch data and R-branch data) are shown in Tables 11–15; these are from the first 10 lines of data.

Table 13
Rovibrational Energy Values for $^3HeH^+$ Computed with Effective Masses

v	J	State Energy (cm^{-1})
0	0	0.000000
1	0	2995.082249
2	0	5663.172987
3	0	8002.114235
4	0	10006.125499
5	0	11665.761640
6	0	12968.796813
7	0	13904.147031
8	0	14475.464693
9	0	14736.893395

Table 14
P-branch Data for $^3HeH^+$ Computed with Effective Masses

v'	J'	v''	J''	*A*-coefficient (s^{-1})	Upper State Energy (cm^{-1})	Lower State Energy (cm^{-1})	Transition Energy (cm^{-1})
1	0	0	1	824.763686	2995.082249	71.369657	2923.712592
1	1	0	2	537.166623	3060.469917	213.668464	2846.801453
1	2	0	3	469.613234	3190.814841	426.020550	2764.794290
1	3	0	4	431.954085	3385.260867	707.124780	2678.136087
1	4	0	5	403.227586	3642.535263	1055.269442	2587.265820
1	5	0	6	377.861281	3960.961962	1468.351007	2492.610955
1	6	0	7	353.837810	4338.478353	1943.896270	2394.582083
1	7	0	8	330.325373	4772.654892	2479.087126	2293.567765
1	8	0	9	306.978662	5260.716669	3070.787089	2189.929580
1	9	0	10	283.679731	5799.565981	3715.568637	2083.997344

Table 15
R-branch Data for $^3HeH^+$ Computed with Effective Masses

v'	J'	v''	J''	*A*-coefficient (s^{-1})	Upper State Energy (cm^{-1})	Lower State Energy (cm^{-1})	Transition Energy (cm^{-1})
0	1	0	0	0.106062	71.369657	0.000000	71.369657
0	2	0	1	1.014328	213.668464	71.369657	142.298807
0	3	0	2	3.644720	426.020550	213.668464	212.352086
0	4	0	3	8.880237	707.124780	426.020550	281.104229
0	5	0	4	17.537466	1055.269442	707.124780	348.144663
0	6	0	5	30.345693	1468.351007	1055.269442	413.081564
0	7	0	6	47.928719	1943.896270	1468.351007	475.545263
0	8	0	7	70.789303	2479.087126	1943.896270	535.190856
0	9	0	8	99.296318	3070.787089	2479.087126	591.699963
0	10	0	9	133.674575	3715.568637	3070.787089	644.781548

ORCID iDs

Paulo H. R. Amaral https://orcid.org/0000-0003-0799-4143
Leonardo G. Diniz https://orcid.org/0000-0001-6994-2045
Alexander Alijah https://orcid.org/0000-0002-4915-0558
Ludwik Adamowicz https://orcid.org/0000-0001-9557-0484
José R. Mohallem https://orcid.org/0000-0002-4776-4417

References

Abgrall, H., Roueff, E., & Viala, Y. 1982, A&AS, 50, 505
Alijah, A., & Duxbury, G. 1990, MolPh, 70, 605
Amaral, P. H. R., & Mohallem, J. R. 2017, JChPh, 146, 194103
Balint-Kurti, G. G., Moss, R. E., Slader, I. A., & Shapiro, M. 1990, PhRvA, 41, 4913
Bernath, P., & Amano, T. 1982, PhRvL, 48, 20
Bethe, H. A., & Salpeter, E. E. 1977, Quantum Mechanics of One- and Two-electron Atoms (New York: Plenum)
Bishop, D. M., & Cheung, L. M 1979, JMoSp, 75, 462
Blom, C. E., Mller, K., & Filgueira, R. R. 1987, CPL, 140, 489
Bunker, P. R., & Moss, R. E. 1977, MolPh, 33, 417
Carrington, A., Buttenshaw, J., Kennedy, R. A., & Softley, T. P. 1981, MolPh, 44, 1233
Carrington, A., Kennedy, R. A., & Softley, T. P. 1983, CP, 81, 251
Carrington, A., Leach, C. A., Marr, A. J., et al. 1992, CP, 166, 145
Carrington, A., Leach, C. A., Marr, A. J., et al. 1993, JChPh, 98, 5290
Carrington, A., McNab, I. R., & Montgomerie, C. A. 1989, JPhB, 22, 3551
Cencek, W., & Kutzelnigg, W. 1997, CPL, 266, 383
Chuang, M.-C., & Zare, R. N. 1987, JMoSp, 121, 380
Coppola, C. M., Lodi, L., & Tennyson, J. 2011, MNRAS, 415, 487
Coxon, J. A., & Hajigeorgiou, P. G. 1999, JMoSp, 193, 306
Crofton, M. W., Altman, R. S., Haese, N. N., & Oka, T. 1989, JChPh, 91, 5882
Diniz, L. G., Alijah, A., Adamowicz, L., & Mohallem, J. R. 2015, CPL, 633, 89
Diniz, L. G., Alijah, A., & Mohallem, J. R. 2012, JChPh, 137, 164316

Diniz, L. G., Alijah, A., & Mohallem, J. R. 2018, ApJS, 235, 35
Diniz, L. G., Kirnosov, N., Alijah, A., Mohallem, J. R., & Adamowicz, L. 2016, JMoSp, 322, 22
Engel, E. A., Doss, N., Harris, G. J., & Tennyson, J. 2005, MNRAS, 357, 471
Esry, B. D., & Sadeghpour, H. R. 1999, PhRvA, 60, 3604
Galli, D., & Palla, F. 1998, A&A, 335, 403
Gonçalves, C., & Mohallem, J. R. 2004, JCoCh, 25, 1736
Güsten, R., Wiesemeyer, H., Neufeld, D., et al. 2019, Natur, 568, 357
Hirshfeld, F. L. 1977, AcTC, 44, 129
Hoyland, J. R. 1967, JChPh, 47, 49
Ishikawaa, A., Nakashima, H., & Nakatsuji, H. 2012, CP, 401, 62
Jiang, S., Yu, C., Yuan, G., Wu, T., & Lu, R. 2017, NatSR, 7, 42086
Jones, K., Formanek, M., Mazumder, R., Kirnosov, N., & Adamowicz, L. 2016a, MolPh, 114, 1634
Jones, K., Kirnosov, N., Sharkey, K. L., & Adamowicz, L. 2016b, MolPh, 114, 2052
Kediziera, D., Stanke, M., Bubin, S., Barysz, M., & Adamowicz, L. 2006, JChPh, 15, 014318
Kolos, W., & Peek, J. M. 1976, CP, 12, 381
Komasa, J., Piszczatowski, K., Ach, G., et al. 2011, J. Chem. Theory Comput., 7, 3105
Korobov, V. I. 2006, PhRvA, 74, 052506
Korobov, V. I. 2008, PhRvA, 77, 022509
Kutzelnigg, W. 2007, MolPh, 105, 2627
Lepp, S., Stancil, P. C., & Dalgarno, A. 2002, JPhB, 35, R57
LeRoy, R. J. 2017, JQSRT, 186, 167
Lillestonen, T. C., & Wheatley, R. J. 2008, ChCom, 45, 5909
Liu, D.-J., Ho, W.-C., & Oka, T. 1987, JChPh, 87, 2442
Liu, Z., & Davies, P. B. 1997a, JChPh, 107, 337
Liu, Z., & Davies, P. B. 1997b, PhRvL, 79, 2779
Matsushima, F., Oka, T., & Tagaki, K. 1997, PhRvL, 78, 1664
Mohallem, J. R., Diniz, L. G., & Dutra, A. S. 2011, CPL, 501, 575
Nakashima, H., Hijikata, Y., & Nakatsuji, H. 2013, ApJ, 770, 144
Nakashima, H., & Nakatsuji, H. 2013, JChPh, 139, 074105
Pachucki, K. 2012, PhRvA, 85, 042511
Pachucki, K., & Komasa, J. 2008, PhRvA, 78, 052503
Pachucki, K., & Komasa, J. 2009, JChPh, 130, 164113
Pachucki, K., & Komasa, J. 2010, PCCP, 12, 9188
Pachucki, K., & Komasa, J. 2012, JChPh, 137, 204314
Patra, S., Karr, J.-P., Hilico, L., et al. 2018, JPhB, 51, 024003
Pavanello, M., Cafiero, M., Bubin, S., & Adamowicz, L. 2008, IJQC, 108, 2291
Perry, A. J., Hodqesl, J. N., Markusl, C. R., Kocherill, G. S., & McCall, B. J. J. 2014, JChPh, 141, 101101
Purder, J., Civis, S., Blom, C. E., & van Hemert, M. C. 1992, JMoSp, 153, 701
Roberge, W., & Dalgarno, A. 1982, ApJ, 255, 489
Rothman, L. S., Jacquemart, D., Barbe, A., et al. 2017, JQSRT, 203, 3
Schmidt, M. W., Baldridge, K. K., Boatz, J. A., et al. 1993, JCoCh, 14, 1347
Shen, J., Borodin, A., Hansen, M., & Schiller, S. 2012, PhRvA, 85, 032519
Sprecher, D., Liu, J., Jungen, C., Ubachs, W., & Merkt, F. 2010, JChPh, 133, 111102
Stanke, M., Palikot, E., & Adamowicz, L. 2016a, JChPh, 144, 174101
Stanke, M., Palikot, E., Kediziera, D., & Adamowicz, L. 2016b, JChPh, 144, 224111
Tennyson, J., Yurchenko, S. N., Al-Refaie, A. F., et al. 2016, JMoSp, 327, 73
Tolliver, D. E., Kyrala, G. A., & Wing, W. H. 1979, PhRvL, 43, 1719
Tung, W.-C., Pavanello, M., & Adamowicz, L. 2012, JChPh, 137, 164305
Wolniewicz, L. 1995, JChPh, 103, 1792
Wolniewicz, L., & Poll, J. D. 1986, MolPh, 59, 953